COBEM 2021 26th International Congress of Mechanical Engineering
November 22-26, 2021, Virtual Congress, Brazil

COB-2021-1878
LASER DIRECTED ENERGY DEPOSITION (L-DED) OF AISI 410L: DEVELOPMENT OF AN OPERATIONAL MAP AND THE EFFECT PROCESSING PARAMETER ON THE BEAD GEOMETRY

Jurandir Marcos Sá de Sousa[1,2]
Jhonattan Gutjahr[1,2]
Anselmo Thiesen Júnior[2]
[1]Universidade Federal de Santa Catarina, Campus Reitor João David Ferreira Lima, s/n°, Trindade-CEP: 88040-900.
[2]Instituto Senai de Inovação em Sistemas de Manufatura e Processamento a Laser, R. Arno Waldemar Dohler, 308 - Santo Antônio, Joinville - SC, 89219-510.
jurandir.sousa@sc.senai.br
jhonattan.gutjahr@sc.senai.br
anselmo.thiesen@sc.senai.br

Henrique Santos Ferreira[2,3]
[3]Universidade do Estado de Santa Catarina, R. Paulo Malschitzki, 200 - Zona Industrial Norte, Joinville - SC, 89219-710.
henrique.santos@sc.senai.br

Milton Pereira[1]
[1]Universidade Federal de Santa Catarina, Campus Reitor João David Ferreira Lima, s/n°, Trindade-CEP: 88040-900.
milton.pereira@ufsc.br

Leandro João da Silva[4]
[4]Universidade Federal de Uberlândia, Av. João Naves de Ávila, 2121, Santa Mônica - CEP: 38408-100.
leandro.js@ufu.br

Abstract. *Martensitic stainless steel has been used in the Oil and Gas (O&G) industry due to its attractive combination of mechanical properties and corrosion resistance. A common application is in valves components with the long lead time to spared parts as a challenge, which could be translated into high costs. In this sense, additive manufacturing (AM) could be a potential solution to overcome this due to its unique ability to produce parts directly from a 3D model. Among several techniques for metal AM, laser-directed energy deposition (L-DED) stands out for its ability to manufacture large components with moderate geometrical complexity. However, to reach the level of maturity to the point of being applied in O&G, the L-DED technique must be fully mastered by users. Aiming to contribute to this field, the present paper deals with the parameter selection task on the L-DED of AISI 410L martensitic stainless steel. The experimental approach can be divided into two stages. Initially, the hardware capabilities (RPM Innovations Inc., model RPMI 535) were assessed, which was called "operational map". Then, in a delimited area within the operational map, the effects of deposition parameters (laser power, travel speed, and powder feedrate) on geometric characteristics of single beads were assessed through a full factorial design of experiments. The results showed expanded maps for higher values of spot size and powder feedrate. The lower limit of the laser power was due to the tendency of lack of fusion, while the upper limit was attributed to the equipment capabilities. The travel speed lower limit was due to process instabilities and the upper limit was the continuous bead formation. About the effect of deposition parameters, travel speed showed a higher impact because for a given laser power and powder feedrate it changes both: energy density and powder amount per unit length. The powder feedrate exhibited more influence on the bead height, while the width was maintained almost the same, keeping the molten pool width similar. Finally, as higher the laser power the higher the bead height and width, with a higher powder catchment for the larger molten pool. Based on the presented results, it can be concluded that AM L-DED has a spread range of bead geometry possibilities by changing the deposition parameters. Further research will be focused on the construction of some preform aiming evaluating the microstructure and mechanical performance.*

Keywords: *O&G industry, metal additive manufacturing, laser directed energy deposition (L-DED), AISI 410L martensitic stainless steel, operational map.*

1. INTRODUCTION

Stainless steels, in general, are a class of alloys whose applicability and industrial recognition are notorious. Within this family, martensitic stainless steels are found, which are alloys with high mechanical resistance, high hardness,

elevated resistance to corrosion in ambient conditions, and low cost when compared to other stainless steel grades, such as austenitic and duplex (Ravi *et al.*, 2013; Saboori *et al.*, 2018). Martensitic stainless steels are indicated for applications such as power transmission system gears and aircraft landing gear, turbine blades, cutlery, plastic molds, and medical devices. The oil and gas industry (O&G) also uses this steel grade in the construction and/or repair of several components, such as high-pressure pipes, valve parts, and oil distillation towers (Aparecida *et al.*, 2021).

Some challenges are faced in the O&G sector when it comes to the manufacture and/or repair of components. Issues such as obtaining complex geometries, the need to keeping a spare parts stock, production breakdowns for the deteriorated components replacement, the specific parts obsolescence, as well as the high costs of the raw material used in these components manufacturing, are some of the obstacles faced by this industry field (Aparecida *et al.*, 2021). Additive Manufacturing (AM - ISO/ASTM 52900, 2015) has been contributing in this regard. Among the metal AM techniques benefits, we highlight the manufacture of single and/or complex geometries parts, manufacture of components on demand, the possibility of manufacturing components in loco, lead time reduction, obtaining near-net shaping components. To summarize, these advantages can be translated into a significant costs reduction (Milewski, 2017; DebRoy *et al.*, 2018). Additive manufacturing by the Laser Directed Energy Deposition (AM L-DED) process possesses a series of attractions, such as meeting all the metal AM processes features, as mentioned above, added to aspects such as the possibility of processing a wide alloys range (in the powder or wire state) and work with functional composition gradients (employing different metallic powders).

Considering the special properties of martensitic stainless steels, benefits of metal AM, and the L-DED process features; the possibility of manufacturing martensitic stainless steel components using the AM L-DED process turns up as an interesting alternative. However, this technique also has disadvantages, such as high levels of thermal gradient and solidification rate, and multiple thermal heating-cooling cycles (DebRoy *et al.*, 2018). Despite their intrinsic attractive properties, martensitic stainless steels are highly susceptible to defects nucleation, such as cracks and deleterious phases precipitation, when subjected to sudden conditions of temperature variation, a factor that makes their processing difficult by techniques such as AM L- DED (Ravi *et al.*, 2013). In this sense, it is necessary to find process optimization tools that allow the manufacture of defect-free components, with adequate geometry, microstructure, and mechanical performance. One way to achieve this goal is by optimizing the AM L-DED parameters.

A design of experiments of the AM L-DED process comprises three steps: single beads (in which it is possible to vary all process parameters at random), single layers (here, suitable hatch spacing are investigated to avoid problems related to lack or excess overlap between single beads) and multilayer geometry (in this, the overlap between layers is evaluated, aiming to mitigate problems with lack of fusion or excess remelting with previously deposited layers). In all these steps, two specific parameter conditions can be desired: higher Production conditions and the other with higher Resolution. Production parameters refer to parameters dedicated to the manufacturing of larger parts and, usually, less geometric precision. In this sense, higher deposition rates are needed, which can be translated into parameters of higher laser spot sizes, powder feedrates, and energy densities. On the other hand, parameters aiming at better Resolution are required for the manufacturing of components with smaller dimensions and greater geometric precision. Here, it is necessary to use lower deposition rates, which is reflected in parameters of lower spot sizes, powder feedrates, and energy densities.

The investigation of these two conditions is important for the manufacturing of components composed of several parts, and in some of them, it may be necessary and/or more interesting to use one or another condition, either due to the dimensions or the required geometric precision. An example is illustrated in Figure 1, where the same preform is presented, however, shows this manufactured with higher Resolution parameters, where there is greater geometric precision, however, the time, efficiency, and consequently the manufacture costs are higher, when compared to the same manufactured preform with higher Production parameters. In this sense, choosing which parameter to use is a trade-off.

Literature on the research of martensitic stainless steels processability by the AM L-DED and investigation of parameters aiming at higher Production and/or Resolution is still poor. In this scenario, this paper presents a method of determining AM L-DED parameters (laser power - P, travel speed - S, and powder feedrate - F), aiming to obtain defect-free single beads (SB) with adequate geometry in two windows: parameters of high Production and high Resolution.

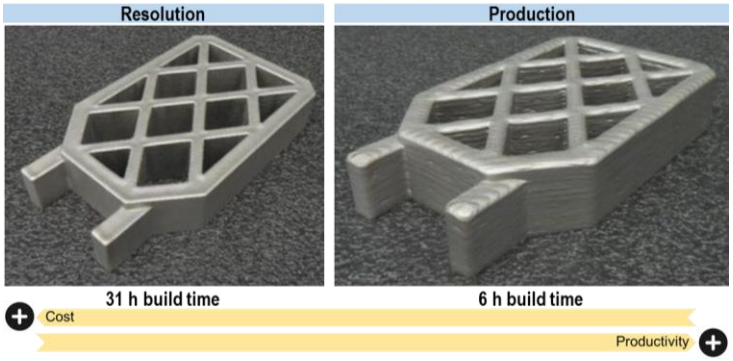

Figure 1. Illustrative example of the difference between Production and Resolution parameters. Inconel 625 preform (no further specification) (Adapted from RPM Innovations Inc., 2017).

2. EXPERIMENTAL APPROACH

2.1 Substrate and feedstock

For the single beads (SB) deposition, AISI 410 martensitic stainless steel substrates in the form of rectangular plates (300.0 x 75.0 x 16.5 mm) were used, provided in the condition of rolled and machined (milled). AISI 410L stainless steel in the powder particle state was employed as feedstock, acquired from Höganäs S/A. The metallic powder was manufactured by the gas atomization process and has a particle size between 53-150 µm. The chemical composition of the substrate (analyzed via Spark-OES, OXFORD), and powder (provided by the manufacturer) are disposed in Table 1.

Table 1. Chemical composition of the AISI 410 substrate and AISI 410L powder.

AISI 410 Substrate										
Spark-OES	Elements (wt.%)	Cr	Mn	Mo	Si	Ni	C	P	S	Fe
		17.5	1.4	0.3	0.3	8.5	0.01	0.03	0.01	Bal.
AISI 410L powder										
Höganäs S/A manufacturer	Elements (wt.%)	Cr	Mn	Si	Ni	C	S	Fe	-	-
		12.2-13.5	0.6-1.0	0.6-1.0	0.1-0.9	0.02-0.03	0.01-0.03	Bal.	-	-

Employing the Field Emission Gun-Scanning Electron Microscope (FEG-SEM, ZEISS SUPRA 55VP), powder morphology was evaluated (see Figure 2a-b). In general, the particles exhibited good circular morphology. At random, powder samples (about 10 g) were prepared for metallographic evaluation (embedding, sanding, and polishing) of cross-section via optical microscope (ZEISS AXIO M2M). These powder particles are illustrated in Figure 2c-d, in which it is possible to perceive the presence of some porosity (with dimensions between 2 and 20 µm) inside the powder particles.

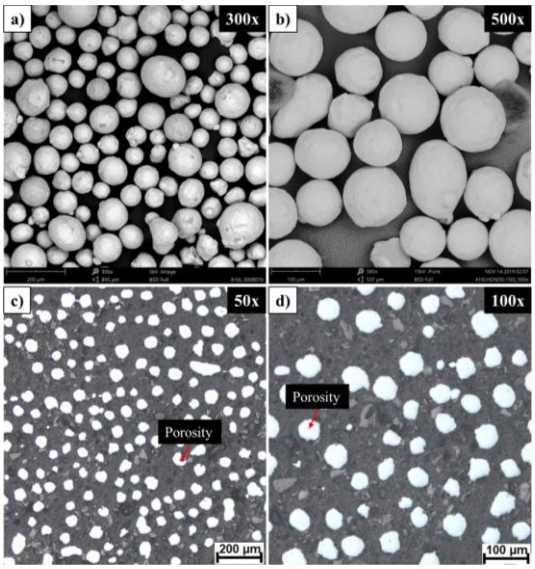

Figure 2. Powder particle morphology captured by FEG-SEM: a) 300x and b) 500x; powder cross-section captured via OM: c) 50x and d) 100x.

2.2 AM L-DED deposition system

The deposition system used was the 5-axis RPMI 535® equipment from RPM Innovations Inc. Argon (Ar) was used as carrier and shielding gas. This machine is coupled to a 3000 W Ytterbium (Yb, YLS-3000-CT) fiber laser source (wavelength [ω] = 1070 nm) from IPG Photonics® manufacturer. A 25° 4-nozzle discrete powder nozzle was employed. The focusing lens and laser fiber diameter (100 µm) can produce a spot size ranging from 0.5 to 3.5 mm.

2.3 SB characterization

SB surfaces images were captured with an optical stereoscope (ZEISS V8). From these images, using Image J software, SB width (w) was measured. SB height (h) was assessed by a vertical height caliper gauge (MITUTOYO). Defects and discontinuities, such as cracks, detachments, and lack of continuity of SB were evaluated visually. Figure 3 summarizes the experimental procedures described in item 2, where 1): prepared AM L-DED system, 2) calibration curve resulting from the powder feedrate flow test, 3) SB as-deposited, 4) SB experimental characterization apparatus.

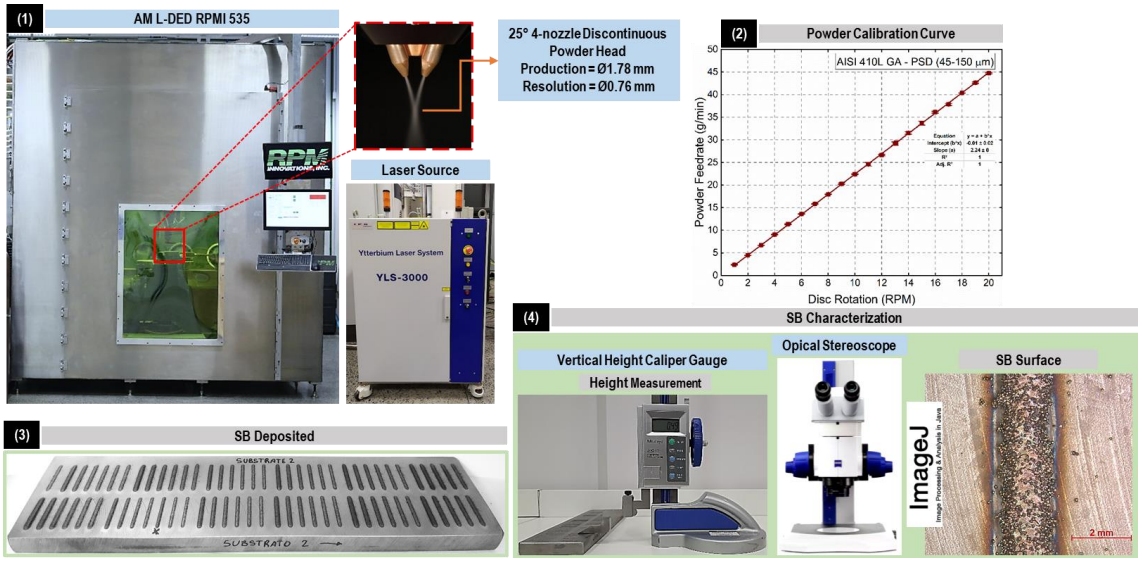

Figure 3. Experimental procedures performed.

2.4 SB deposition process

Substrates were subjected to an abrasive blasting process (IEPCO PEENMATIC® 620, steels shot S70), aiming to remove impurities and make the surface opaque. The AISI 410L powder was previously conditioned in beakers and placed in an oven at 80 °C for 4 h to remove moisture. Powder flow tests were performed: only the powder supplier system of the AM L-DED machine was turned on at a given disk rotation speed for 1 min. After stabilization, using zip-locked plastic bags, the powder was collected at the feeding nozzle outlet, and weighed on a precision scale (0.001 g, MARTE). This procedure was performed, in triplicate, for all integer values of disk rotation, to draw a calibration curve (Figure 3).

Two designs of experiments were performed. First, a parameter matrix was elaborated, keeping the powder feedrate (F) constant and varying the laser power (P) and travel speed (S) at reasonable levels, until a process instability condition is reached, in which SB are no longer formed. Based on this premise, we adopted the method illustrated in the color mosaic (Figure 4), inspired by the works of Da Silva *et al.* (2019) and Mazzucato *et al.* (2019). As fixed parameters, the spot size is highlighted first. As aforementioned, this work aims to identify two parameters windows that allow processing the AISI 410L. In this sense, two different spot sizes were used, Ø = 1.78 mm (Production parameters, aiming to obtain high deposition rates) and Ø = 0.76 mm (Resolution parameters, aiming to obtain high geometric accuracy). The following parameters were also kept fixed in both windows: nozzle setup (coaxial discontinuous - 25°), stand-off distance (0.95 mm), carrier gas (Ar - 6 l/min), and shielding gas (Ar - 40 l/min). From this preliminary study (Figure 4), Production and Resolution windows (regions highlighted in green) for the deposition of definitive SBs were determined, composing the second stage of the design of experiments.

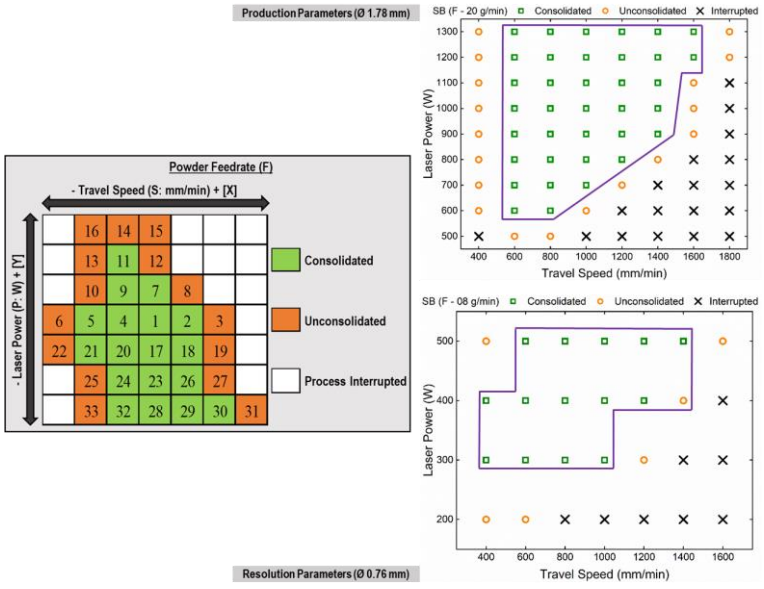

Figure 4. Selection method of the preliminary.

2.5 SB selection methodology

The first steps were to perform visual macro analysis on optical stereoscopy (OS). The SB *h* measurement was performed on a table with a high degree of flatness and with the aid of a vertical height caliper gauge, at 3 different points of the SB. In this stage, all SBs that exhibited cracks, detachments, lack of continuity were eliminated. The *h*, and aspect ratio (*AR*) were quantitative elimination parameters. Due to the high level of parallax error, only in cases where the wettability angle (Θ) is <90°, more attention was paid. In this sense:

- Presence of cracks, detachments, and lack of continuity of SB was assessed visually from the OS images.
- Height (*h*): it was calculated, for each F value, a general *h* mean. SBs that did not reach at least 90% of this value were discarded (see Eq. (1)).

$$h \geq 90\% * \bar{h}\ (mm) \tag{1}$$

- Aspect ratio (*AR*): it was calculated through a direct relationship between the *w* (measured with the aid of the vertical height caliper gauge and software Image J), and *h* of the SB according to Eq. (2). SB that exhibited values ≤2.5±5% were disqualified, due to the tendency that very low *AR* SB have problems in the interface (hatch spacing) of the post single layers deposition, such as porosity and voids insertion (Campanelli *et al.*, 2017).

$$AR = w/h \geq 2.5\ (\text{mm}) \tag{2}$$

- Wettability angle (Θ): Equation 3 was used, from which, in possession of the SB *h* and *w* values, it was possible to project this geometric characteristic (Ocelík *et al.*, 2007). In the present study, it was only decided to disqualify the SB that exhibited Θ <90°±5%.

$$\Theta = 180 - 2 * arctan(2 * h/w)(°) \tag{3}$$

3. RESULTS AND DISCUSSION

It is important to mention that the geometric SB characteristics are unique to them, and may not directly reflect the geometric aspects of the SB hatch spacing step, forming single layers (Ansari *et al.*, 2016). Results are subdivided according to the parameters window (Production and Resolution).

3.1 Production parameters

Observing the 20 g/min window (Figure 5a), one notices a wide region with processability, and the entire range of 700-1300 W and 600-1000 mm/min presented SB classified as good. Only from 1200 mm/min, the problem of low SB *h* started, compromising the rest of the window. For the 25 g/min window (Figure 5b), a large suitable region was also noted. However, from 1000 mm/min S, low SB *h* was identified, concentrated in the regions of lower P. However, advancing on the S axis, this problem expanded towards the higher P ranges, so that the 1600 mm/min range was totally compromised. Besides, a portion of the S ranges between 600 and 1000 mm/min exhibited *AR* less than 2 (w/h<2). The 30 g/min window (Figure 5c) showed a more heterogeneous behavior, making it difficult to define an acceptable region. Here, regarding the low SB *h*, it is noted that this problem became evident only from the 1400 mm/min S, whereas, in the previous window, 1000 mm/min S range already exhibited this problem. Furthermore, some isolated parameters towards the highest P ranges showed acceptable SBs, indicating that the evaluated regions are not yet fully compromised.

Regarding the low SB *h*, the driving causes are the low powder amount per unit length and the shorter interaction time laser beam/powder/substrate, as this problem was noticed only in the higher travel speeds, being S>1200 mm/min for F - 20 g/min and S>1400 mm/min for F - 25 and 30 g/min, respectively. In this sense, the higher S lead to less capture and fusion of powder particles by the molten pool, resulting in lower SB *h*. As for the *AR*<2, this problem may be due to the greater powder amount per unit length, given its predominant presence in the lower S ranges, being 600-800 mm/min S for 25 g/min, 800-1000 mm/min S for the 30 g/min, and the non-observation of this problem in the lowest F - 20 g/min evaluated. Some SBs of the F - 25 and 30 g/min windows exhibited wettability angle lower than 90° (Θ<90°), a characteristic considered prohibitive for the hatch spacing stage, due to the imminent appearance of pores and/or lack of fusion between SBs. Here, it is noteworthy that the Θ was estimated from a geometric relationship based on the *h* and *w* values of the SB, which generate results significantly close to those of experimental procedures for direct measurement of Θ. In this sense, all parameters in which this problem was detected also presented *AR*<2, which denotes the correlation between *AR* and Θ. Figure 6 displays the regression functions obtained from the geometric SB characteristics for the F - 20, 25, and 30 g/min windows, respectively.

Evaluating the process windows (Figure 5) and the regression functions (Figure 6), it is possible to infer that the results are consistent with the literature descriptions. Regarding the SB *h*, it is reported that all parameters (P, S, and F) directly affect this feature, and that minimum energy input is required to ensure the fusion of all particles added for a given P/S

set. In summary, for a given constant F, SB *h* tends to reduce as P decreases and S increases (Toyserkani *et al.*, 2003; Davim, 2008; Barekat *et al.*, 2016; Bax *et al.*, 2017; Aghili and Shamanian, 2019). Concerning SB *AR*, as observed in the calculation relationship, this geometric feature is directly dependent on the SB *w*, which is the equation denominator. In this sense, the literature indicates that P and S exert greater influence on this characteristic when compared to F. An increase in the latter promotes higher absorption of laser beam energy by the particles, which tends to reduce the heat input and consequently the SB *w*, behavior benefited by higher S, due to the shorter interaction time laser beam/powder particles/substrate (Davim, 2008; Aghili and Shamanian, 2019). The SB *w* is directly dependent on P, followed by S, while F shows less significance (Kou, 2003). Following this research line, the behavior of the lowest S ranges was consistent, which indicates that the SB *h* (equation numerator) was the characteristic most benefited by F increase. However, literature also indicates that P exerts a direct influence on the SB *w*, regardless the values of S and F used. This effect is due to the molten pool kinetics, governed by convective currents, such as the Marangoni forces, which can promote the formation of wider SBs (Kou, 2003; Ansari *et al.*, 2016; Barekat *et al.*, 2016). Thus, it is possible to infer that all parameters affect the *AR* behavior (Pinkerton *et al.*, 2008; Lusquiños *et al.*, 2009; Abioye *et al.*, 2013). However, as aforementioned, by F increasing, a greater portion of the laser beam energy incident is absorbed by the powder particles, reducing the heat input on the substrate and SB *w*. Based on the behavior of the F - 25 and 30 g/min windows, this appears to be the most likely cause. The Θ, measured as the tangent angle between the SB surface and substrate, indicates the flatness degree between substrate and SB surface and should be high enough to avoid porosity between passes and ensure lateral overlap between SB. Different descriptions are found as to what is an ideal value of Θ. In general, Θ<90° is considered worrying. The larger the Θ and lower the *AR*, the closer the SB gets to a semi-spherical shape. In these cases, even if Θ>90°, a gap is formed at the base between SB and substrate. During the hatch spacing stage, it is more difficult for the material to drain into these regions, filling them (Oliveira, 2007; Abioye *et al.*, 2013; Barekat *et al.*, 2016; Aghili and Shamanian, 2019). Regarding deposition parameters influence, there is a trend similar to *AR*, with an Θ rise proportional to the increase in P and S, coupled with lower F (Paul *et al.*, 2007). Figure 7 exemplifies SBs from the Production window, classified as good and with reported problems.

For Production parameters, the F - 25 g/min window was elected as the most suitable for the following steps of an AM L-DED processing route, such as the deposition of layers (hatch spacing) and multilayer geometries. The F - 20 g/min window also displayed a lot of parameters rated as good. However, in the latter, the processable region is concentrated in lower S ranges. This factor, added to its lower F, results in lower productivity concerning the 25 g/min window.

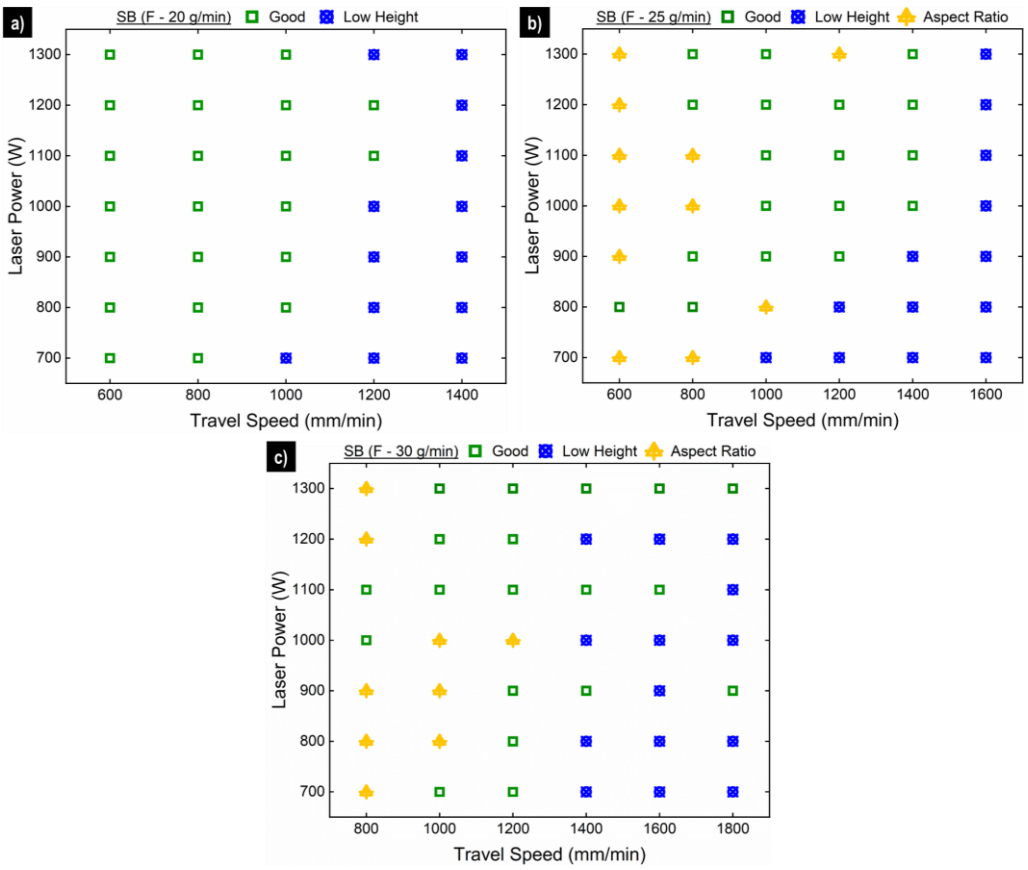

Figure 5. Process windows for Production parameters: a) F - 20 g/min, b) 25 g/min and c) 30 g/min.

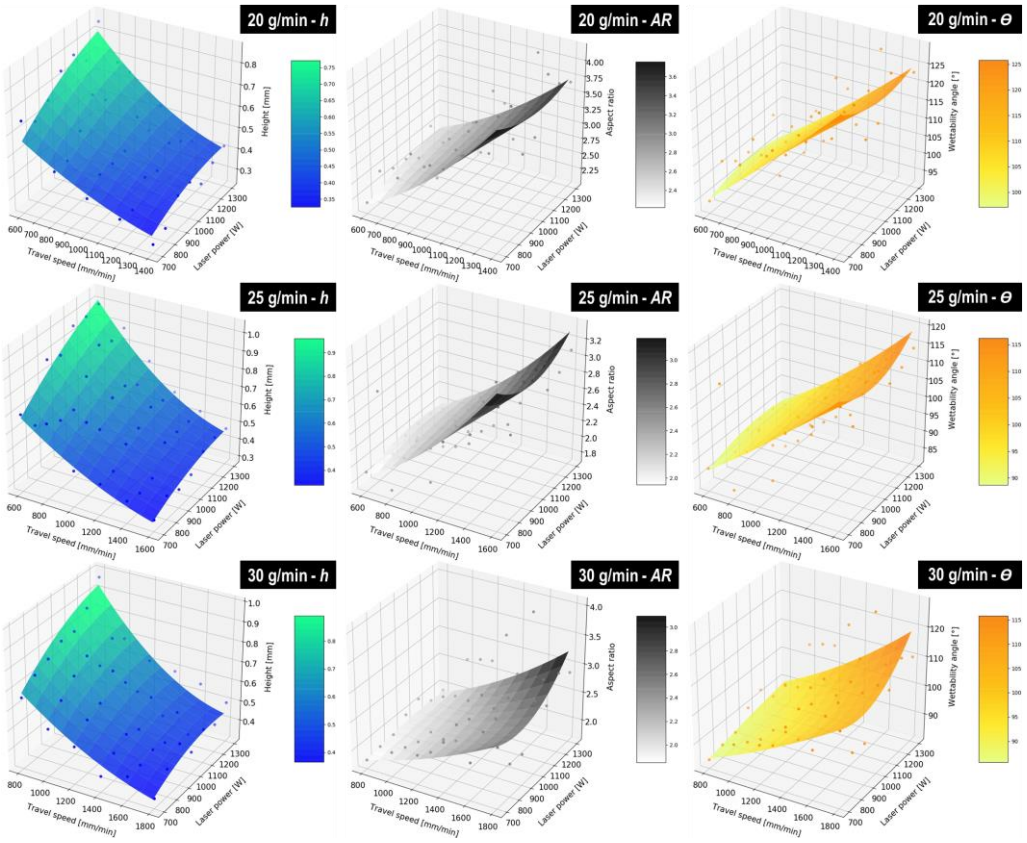

Figure 6. Regression functions for the Production parameters.

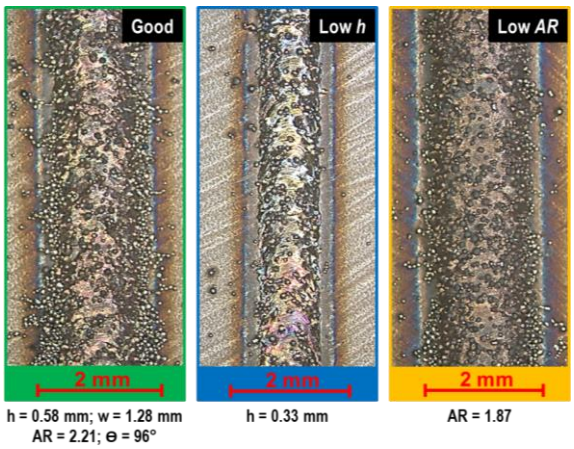

Figure 7. Examples of SB classified as Good and with problems in the Production parameters.

3.2 Resolution parameters

The F - 08 g/min window (Figure 8a) presented processability, however, in a restricted range. For the entire P range, only the 400-800 mm/min showed SB classified as good. Two parameters in the 300 W P range showed low SB *h*. In the 500 W P range, all parameters from 1000 mm/min S exhibited *AR* outside acceptable limits. However, here, unlike the trends seen in the Production windows, *AR* values, mostly stayed well above 2 (w/h>>2), with an overall mean of *AR*>5.0. This pattern was identified in the higher S ranges, while some parameters in the lower S ranges exhibited an *AR*<2. In the F - 12 g/min (Figure 8b), virtually the entire 600-1200 S mm/min range resulted in acceptable SB. From the 1400 mm/min S range, all parameters generated low SB *h*. On the other hand, in the lower 400 mm/min S range, SB with *AR*<2 were observed. For the F - 16 g/min (Figure 8c), a wide processability region was achieved, being that the entire P range of 300-500 W and S between 600-1000 mm/min showed acceptable SB. The lower 400 mm/min S range, in turn, presented *AR*<2. From 1200 mm/min S, all SBs exhibited low *h*, so that only the 500 W P range exhibited proper behavior.

Regarding the low SB *h*, the low F, associated with S increase can be indicated as justifications for this behavior, which resulted in less powder amount per unit length, directly contributing to the low SB *h* generation. As highlighted, this problem was noticed only in the greater travel speeds, being S>1400 mm/min for F - 12 g/min and S>1200 mm/min for F - 16, respectively. In this sense, the higher S lead to less capture and fusion of powder particles by the molten pool, resulting in lower SB *h*. For the F - 08 g/min window, this problem presented an outlier characteristic, in an undefined region. As for the *AR*<2, this problem may be due to the greater powder amount per unit length, given its predominant presence in the lower 400 mm/min S range for F - 12 and 16 g/min, respectively, and the non-observation of this problem in the lowest F - 08 g/min evaluated. Concerning the very high *AR* problem, the same was identified only in the lowest windows of F - 08 and 12 g/min and in the higher S ranges, being 1200 mm/min for F - 08 g/min and in a single parameter of the 1200 mm/min S range. This behavior can be attributed to the excessive *w* increase concerning the SB *h*, which provides an opposite effect to that observed in the parameters with higher *AR*. The laser beam/powder beam/substrate interaction was altered, which may be generating a higher direct heat input into the substrate, thus increasing the effect of the Marangoni convection currents acting in the molten pool. Confirming this trend, only the AR<2 parameters exhibited Θ<90°. Figure 9 displays the regression functions obtained from the geometric SB characteristics for the F - 08, 12, and 16 g/min windows, respectively.

Evaluating the process windows (Figure 8) and the regression functions (Figure 9), it is possible to infer that the results are consistent with the literature descriptions. Regarding the SB *h*, AR<2, and Θ<90°, the trends observed were the same as those described in the Production parameters. However, here, in the Resolution ones, it is worth noting that narrower windows were investigated, precisely because of the lower spot size used, which makes the laser beam energy distribution more concentrated and limits the ranges of F, P, and S available. Concerning SB *AR* parameters much higher than 2, as aforementioned, this geometric feature is directly dependent on the SB *w*. Thus, the lowest F windows and the largest S ranges analyzed provided greater heat input into the substrate, increasing the SB *w*, inverting the calculation ratio results. Figure 10 exemplifies SBs from the Resolution window, classified as good and with reported problems.

In this sense, for Resolution parameters, the F - 16 g/min window was elected as the most suitable for the following steps of an AM L-DED processing route, such as the deposition of layers (hatch spacing) and multilayer geometries. Besides that, the F - 12 g/min window also seems a feasible option.

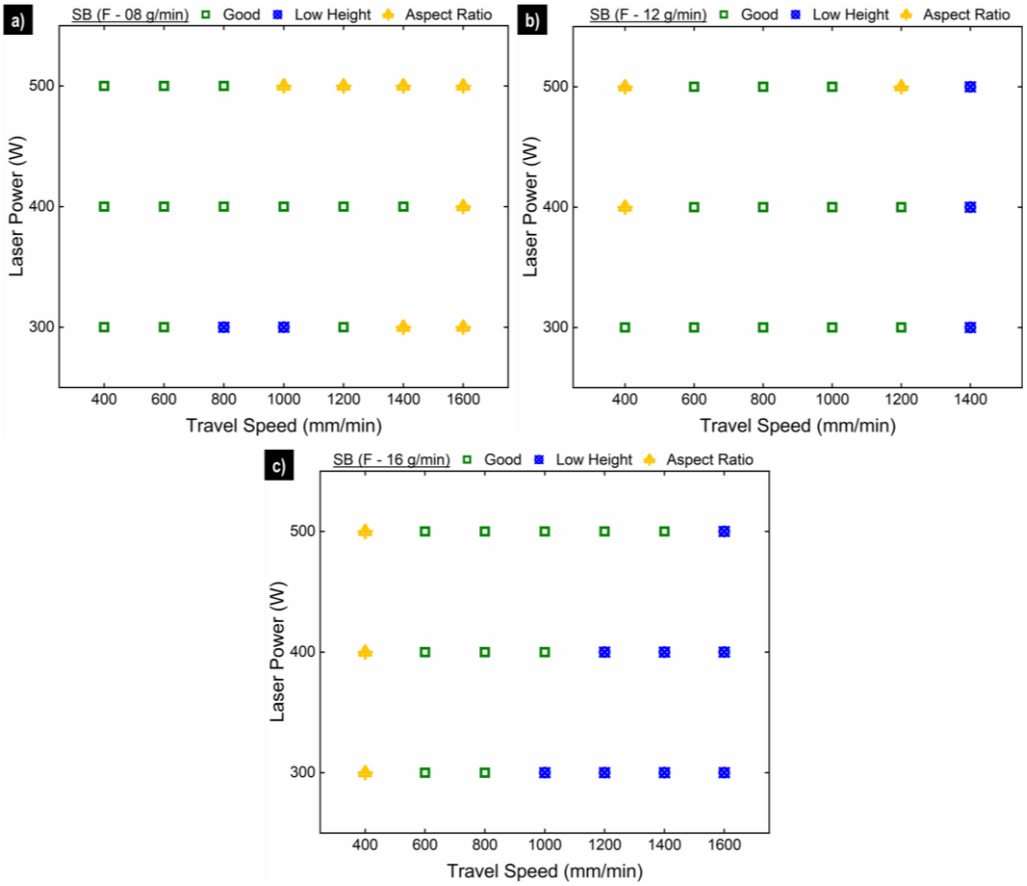

Figure 8. Process windows for Resolution parameters: a) F - 08 g/min, b) 12 g/min and c) 16 g/min.

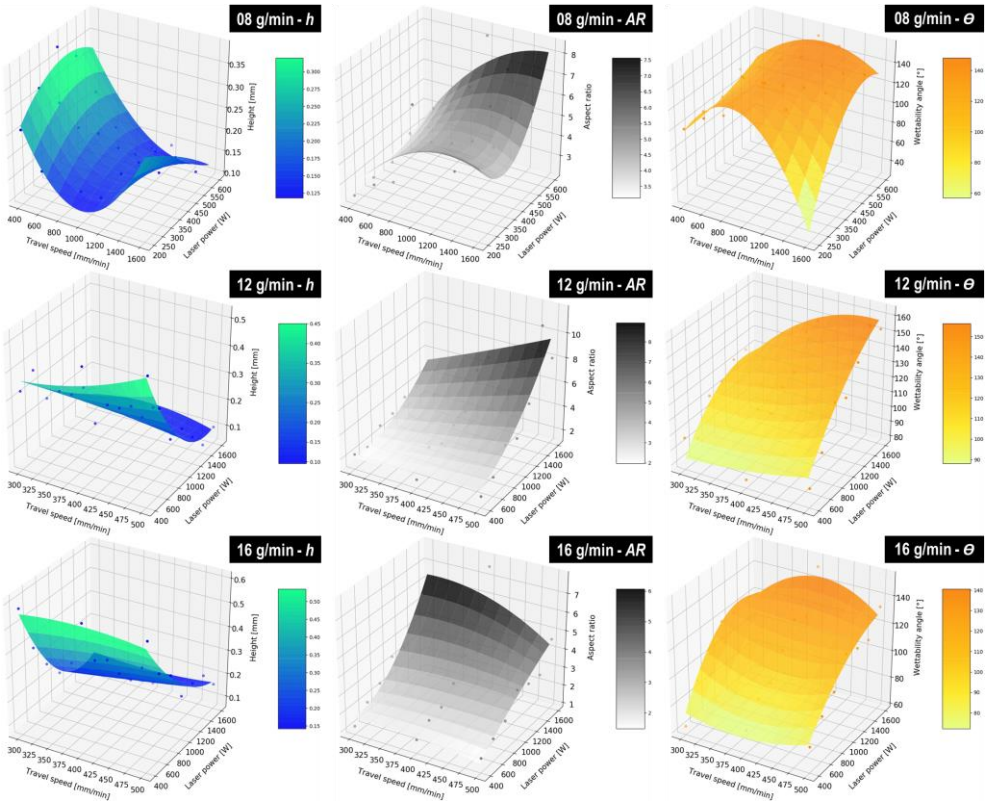

Figure 9. Regression functions for the Resolution parameters.

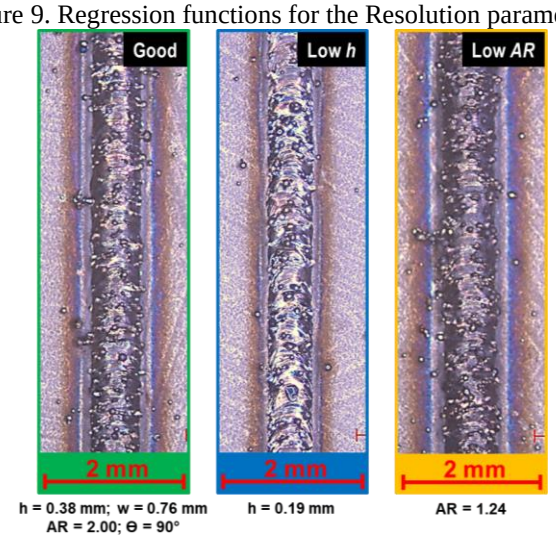

Figure 10. Examples of SB classified as Good and with problems in the Resolution parameters.

4. CONCLUSIONS

This work presented an exploratory study aiming to identify the processability windows and limits to single beads (SB) deposition. The main AM L-DED process parameters (P, S and F) were varied. Some conclusions can be inferred:

- Regarding the Production parameters, it was observed that the lower F windows showed larger processable ranges. In the lower S ranges, good SBs were obtained for the lower F, however, there is a trend of low SB *AR* for the higher F. In the greater S ranges, low SBs *h* were formed.
- In the Resolution parameters, it was observed that the higher F windows presented larger processable ranges. The observed trends were analogous to the Production parameters, however, in more restricted ranges, due to the energy density concentration increasing, provided by the lower spot size.
- F increase was interesting only up to a certain limit, after which no significant gains in productivity were observed. It was also possible to notice an instability in the process above a certain energy density. This limit showed higher sensitivity in the Resolution parameters. On the other hand, very low energy densities did not form suitable SBs.

5. ACKNOWLEDGEMENTS

Thanks to Instituto Senai de Inovação em Sistemas de Manufatura e Processamento a Laser (ISI-LASER, Brazil) for the technical-scientific support. Thanks also to Universidade Federal de Santa Catarina (UFSC, Brazil) and Universidade Federal de Uberlândia (UFU, Brazil) for their scientific support.

6. REFERENCES

Abioye, T. E., Folkes, J. and Clare, A. T., 2013, "A parametric study of Inconel 625 wire laser deposition," *J. Mater. Process. Technol.*, vol. 213, no. 12, pp. 2145–2151, doi: 10.1016/j.jmatprotec.2013.06.007.

Aghili, S. E., and Shamanian, M., 2019, "Investigation of powder fed laser cladding of NiCr carbides single-tracks on titanium aluminide substrate," *Opt. Laser Technol.*, vol. 119 p. 105652, doi: 10.1016/j.optlastec.2019.105652.

Ansari, M., Shoja Razavi, R. and Barekat, M., 2016, "An empirical-statistical model for coaxial laser cladding of NiCrAlY powder on Inconel 738 superalloy," *Opt. Laser Technol.*, vol. 86, pp. 136–144, doi: 10.1016/j.optlastec.2016.06.014.

Aparecida, K., Barcelos, M., De Faria, G. L., Humberto, R., and De Siqueira, M., 2021, "Heat treatment effects on the hardness and wear behavior of laser-welded AISI40 martensitic steel plates", *Int. J. of Adv. Man. Technol.*, vol. 114, pp. 1155–1163, doi: 10.1007/s00170-021-06942-6.

Barekat, M., Shoja Razavi, R. and Ghasemi, A., 2016, "Nd:YAG laser cladding of Co-Cr-Mo alloy on γ-TiAl substrate", *Opt. Laser Technol.*, vol. 80, pp. 145–152, doi: 10.1016/j.optlastec.2016.01.003.

Bax, B., Rajput, R., Kellet, R. and Reisacher, M., 2017., "Systematic evaluation of process parameter maps for laser cladding and directed energy deposition," *Addit. Manuf.*, vol. 21, June 2017, pp. 487–494, doi: 10.1016/j.addma.2018.04.002.

Campanelli, S. L., Angelastro, A., Signorile, C. G. and Casalino, G., 2017, "Investigation on direct laser powder deposition of 18 Ni (300) marage steel using mathematical model and experimental characterisation," *Int. J. Adv. Manuf. Technol.*, vol. 89, no. 1–4, pp. 885–895, doi: 10.1007/s00170-016-9135-x.

Davim, J.P., Oliveira, C. and Cardoso, A., 2008, "Predicting the geometric form of clad in laser cladding by powder using multiple regression analysis (MRA)," *Mater. Des.*, vol. 29, no. 2, pp. 554–557, doi: 10.1016/j.matdes.2007.01.023.

Da Silva, L.J., 2019. "Near-Immersion Active Cooling for Wire + Arc Additive Manufacturing: From Concept To Application Near-Immersion Active Cooling for Wire + Arc Additive", Doctoral Thesis, Graduate Program in Mechanical Engineering, Federal University of Uberlândia, Uberlândia, Brazil.

DebRoy, T., Wei, H. L., Zuback, J. S., Mukherjee, T., Elmer, J. W., Milewski, J. O., Beese, A. M., Wilson-Heid, A., De, A., Zhang, W., 2018, "Additive manufacturing of metallic components – Process, structure and properties," *Prog. Mater. Sci.*, vol. 92, pp. 112–224, doi: 10.1016/j.pmatsci.2017.10.001.

ISO/ASTM 52900, "Standard Terminology for Additive Manufacturing – General Principles – Terminology,", 2015, *ASTM International*. International Organization for Standardization/American Society for Testing and Materials, Pennsylvania, pp. 1–9. Available: http://compass.astm.org/EDIT/html_annot.cgi?ISOASTM52900+15.

Kou, S., *Welding metallurgy*, 2003, 2nd ed. Hoboken: John Wiley & Sons, Inc.

Lusquiños, F., Comesaña, R., Riveiro, A., Quintero, F. and Pou, J., 2009, "Fibre laser micro-cladding of Co-based alloys on stainless steel," *Surf. Coatings Technol.*, vol. 203, no. 14, pp. 1933–1940, doi: 10.1016/j.surfcoat.2009.01.020.

Mazzucato, F., Aversa, A., Doglione, R., Biamino, S., Valente, A. and Lombardi, M., 2019, "Influence of Parameters and Deposition Strategy on Laser Metal Deposition of 316L," *Metals*, vol. 9, no. 11, p. 1160, doi: 10.3390/met9111160.

Milewski, J. O., *Additive manufacturing of metals: From fundamental technology to rocket nozzles, medical implants, and custom jewelry*, 2017, 1st ed., vol. 258. Santa Fe, NM: Springer.

Ocelík, V., De Oliveira, U., De Boer, M. and De Hosson, J. T. M., 2007, "Thick Co-based coating on cast iron by side laser cladding: Analysis of processing conditions and coating properties," *Surf. Coatings Technol.*, vol. 201, no. 12, pp. 5875–5883, doi: 10.1016/j.surfcoat.2006.10.044.

Paul, C. P., Ganesh, P., Mishra, S. K., Bhargava, P., Negi, J. and Nath, A. K., 2007, "Investigating laser rapid manufacturing for Inconel-625 components," *Opt. Laser Technol.*, vol. 39, no. 4, pp. 800–805, doi: 10.1016/j.optlastec.2006.01.008.

Pinkerton, A. J., Wang, W. and Li, L., 2008, "Component repair using laser direct metal deposition," *Proc. Inst. Mech. Eng. Part B J. Eng. Manuf.*, vol. 222, no. 7, pp. 827–836, doi: 10.1243/09544054JEM1008.

Ravi, G. A., Hao, X. J., Wain, N., Wu, X., and Attallah, M. M., 2013, "Direct laser fabrication of three dimensional components using SC420 stainless steel," *Mater. Des.*, Vol. 47, pp. 731–736, doi: 10.1016/j.matdes.2012.12.062.

RPM Innovations Inc., 2017, "RPMI 535 Operations Manual", 143 p.

Saboori, A., 2018, "Accelerated Process Parameter Optimization for Directed Energy Deposition of 316L Stainless Steel" *Eur. Powder Metall. Assoc.*, doi: 10.3390/app7090883.

Toyserkani, E., Khajepour, A and Corbin, S., 2003, "Three-dimensional finite element modeling of laser cladding by powder injection," *J. Laser Appl.*, vol. 15, no. 3, pp. 153–160, doi: 10.2351/1.1585087.

7. RESPONSIBILITY NOTICE

The authors are the only responsible for the printed material included in this paper.